Journal of Power Sources 191 (2009) 601–613

Contents lists available at ScienceDirect

Journal of Power Sources

journal homepage: www.elsevier.com/locate/jpowsour

Effect of nanoscopic confinement on improvement in ion conduction and stability properties of an intercalated polymer nanocomposite electrolyte for energy storage applications

Saumya R. Mohapatra, Awalendra K. Thakur*, R.N.P. Choudhary

Department of Physics & Meteorology, Indian Institute of Technology (I.I.T.), Kharagpur 721302, India

ARTICLE INFO

Article history:
Received 25 September 2008
Received in revised form 5 January 2009
Accepted 19 January 2009
Available online 13 February 2009

Keywords:
Intercalated nanocomposite
Thermal stability
Complex impedance spectroscopy
Voltage stability
Ion transport
Electrochemical power source

ABSTRACT

Nanoscopic confinement of a cation coordinated polymer in the channels of organo-modified montmorillonite clay results in substantial improvement in conductivity, cation transport and stability properties required for energy storage/conversion devices. X-ray diffraction analysis confirms composite formation as evidenced by: (i) intercalation of PEO_8–$LiClO_4$ into the clay channels for clay loading ≥7.5 wt.% and (ii) partial intercalation/exfoliation for a lower clay loading (≤5 wt.%). Transmission electron microscopy analysis corroborates these findings as indicated by an enhancement in clay gallery width from 6 to 9 Å for 20 wt.% clay providing evidence for intercalation at higher clay loadings. Energy dispersive X-ray dot-mapping images confirm the homogeneous distribution of clay in nanocomposites. Thermal analysis indicates a strong dependence of thermodynamic parameters, e.g., glass transition (T_g), crystalline melting (T_m), melting enthalpy, glass transition width (ΔT_g), and thermal relaxation strength (ΔC_p), on clay concentration. These observations agree well with changes in electrical properties on nanocomposite formation. Substantial enhancement in ambient conductivity (~208 times) occurs in a nanocomposite film (2 wt.% clay) relative to a clay-free film. The temperature dependence of conductivity obeys Arrhenius behaviour below T_m and the VTF (Vogel–Tamman–Fulcher) relationship above T_m. The ionic transport number (~99.9%) confirms ionic charge transport with a cation contribution (t_{Li^+}) ~ 0.5 for 2 wt.% clay. It represents an increase by ~65% in comparison with PEO_8–$LiClO_4$. Improvement in voltage and thermal stability is also observed with the nanocomposites.

1. Introduction

Ion-conducting polymers have drawn considerable attention for more than a decade in view of their potential application in ionic devices such as high specific energy solid-state batteries, supercapacitors, and proton-exchange membrane fuel cells. An ion-conducting solid polymer film has the ability to function both as the separator and an electrolyte in storage devices unlike the case of present-generation Li-ion cells. Due to this, the development and scaling-up of the properties of ionically conducting solid polymer membranes, conventionally known as solid polymer electrolytes (SPEs), is considered attractive and challenging. It has always been an important and highly competitive research and development activity due to the stringent requirements of the material parameters driven by the application criteria and the high-end commercial value of the SPEs for electrochemical power sources. As a consequence, there has been a pressing demand for the development of a suitable ion-conducting polymer based separator along with the parallel development of electrode materials for application in energy-conversion/storage devices.

Inherent deficiencies of stability and ambient conductivity have been identified as the major drawback of SPEs. The primary factors that imposed severe restraint on the applicability of ion-conducting polymer films in devices are: (i) low ambient ionic conduction; (ii) concentration polarization; (iii) poor stability properties (thermal, electrochemical, mechanical interfacial, etc.). One of the major reasons for poor ionic conductivity and concentration polarization has been attributed to possibility of an ion-association (ion-pairing) effect [1]. It arises due to columbic interaction between cations and anions in the solid polymer matrix. This is because the mobile charges in the polymer-based ion-conducting films originate due to dissociation of cations (M^+) and anions (X^-) of the salt (MX) in the host polymer, having weak permittivity (~3–5), swollen into a volatile polar organic solvent. Thus there is a high probability of ions remaining both as free charges (cation/anion) and ion-pairs [2–4]. Ion-pair formation can cause concentration polarization and immobilization of conducting species whenever an excess number of ion-pairs are present in the host polymer matrix in comparison

* Corresponding author. Tel.: +91 3222 283834; fax: +91 3222 255303.
E-mail address: akt@phy.iitkgp.ernet.in (A.K. Thakur).

0378-7753/$ – see front matter © 2009 Elsevier B.V. All rights reserved.
doi:10.1016/j.jpowsour.2009.01.100

with the available number (fraction) of free-charge carriers (i.e., the anions and hence the cations). The overall effect is a lowering in electrical conductivity that imposes serious limitations on the suitability of SPEs for devices. This has therefore prompted the search for new alternative materials with superior properties.

A number of approaches have been proposed to solve the state-of-the-art problems of ion-conducting polymers [5,6]. Nanocomposite formation is the latest suggestion. Polymer nanocomposite (PNCE) films formed via the intercalation of cation-coordinated polymers in the nanometric channels of inorganic clay (e.g., montmorillonite, zeolite etc.) have drawn considerable attention in recent years. They are known as "intercalation nanocomposites". The intercalation of an ion-conducting polymer–salt (PS) complex in the nanometric channels of an organo-modified clay such as montmorillonite, which is endowed with an organophilic property on modification, is considered effective in minimizing the ion-pairing effect. The central idea is based on the concept that organic modification of the clay causes an accumulation of negative charge on its surface and thereby restricts the entry of bulky anions into the nanometric channels (galleries). On the other hand, clay galleries develop a capability for accommodating cation-coordinated polymer chains favoured by Coulombic interaction. In view of this, the intercalation approach of nanocomposite formation appears to be a novel procedure [7,8] to overcome existing challenges with polymer-based ionic conductors. In addition, this approach seems to be attractive with definite scope to minimize concentration polarization (i.e., to reduce ion-pairing) due to an effective separation between the cations and anions on nanoscopic confinement of the ion-coordinated polymer chains into the clay channels.

Aranda and Hitzky [9] first attempted nanocomposite formation by direct intercalation of an insulating polymer, polyethylene oxide (PEO), into montmorillonite (MMT) clay. They succeeded in intercalation without any significant achievement of the desirable properties (e.g., conductivity) of the nanocomposite for applications in devices under ambient conditions. Subsequently, Giannelis and co-workers [7,8,10–12] explored the possibility of intercalation on the basis of thermodynamical free energy considerations and simulation studies to investigate the conformational and structural arrangement of polymer chains between successive clay layers. They observed that the intercalation of a cation-coordinated polymer chain via an ion-exchange reaction is easier than intercalating pure PEO. Following these reports in the literature, a large number of smectic clays such as montmorillonite [5–9], hectorite [13,14], and laponite [15] have been used for composite formation in combination with different polymers. Of these, montmorillonite is still a favoured choice in view of its special features of high aspect ratio (∼1000), high cation-exchange capacity (CEC ∼ 80 meq/100 g), large specific surface area (∼31.82 $m^2\,g^{-1}$), appropriate interlayer charge (∼0.55) and length scale (clay channel width ≡ 16 Å). Nevertheless organo-modification of the clay is an essential prerequisite to make it organophilic [2] in order to achieve the desirable features in the material system to be fabricated.

Recently, Kim et al. [16] reported composite formation of a plasticized polymer electrolyte ($PEO_{16}LiClO_4$ + 50 wt.% EC) with tallow modified Na-MMT. They observed an optimum value of room temperature conductivity of $\sim10^{-5}\,S\,cm^{-1}$ for the plasticized electrolyte and $\sim10^{-4}\,S\,cm^{-1}$ for the composite (10 wt.% modified MMT). Fan et al. [17] studied composite formation with combination of organo-modified Li-MMT/Na-MMT and $PEO_{16}LiClO_4$. They reported an enhancement in conductivity at room temperature by 30 times for the composite polymer film ($\sim3.5\times10^{-6}\,S\,cm^{-1}$) in comparison with that of pure $PEO_{16}LiClO_4$ ($\sim1.2\times10^{-7}\,S\,cm^{-1}$). These reports could not, however, cover a number of scientifically and technologically important aspects such as the stability (thermal, voltage), ion transport properties and confirmation of the phase structure (i.e., intercalation) of the composite polymer film. In addition, the ambient conductivity is still far below the desirable value for device application. Further, use of a plasticizer is normally expected to degrade the stability of solid polymer films. The problem of relatively lower ambient conductivity in the above studies may be related to the selection of the polymer–salt stoichiometric ratio. Literature reveals that an optimized ratio of Ö/Li ≡ 8:1 represents a eutectic composition in the case of a PEO:$LiClO_4$ complex that shows maximum conductivity and a lower crystalline melting point (T_m) [18,19].

Based on these reports, the present experimental investigation has been conducted with emphasis on analyzing the properties of polymer nanocomposite films to judge their suitability for application in energy storage/conversion devices. The work aims to demonstrate a practical approach to overcome the inherent problems of ion conducting solid polymer films by means of nanoscopic confinement of an optimized combination of a Li^+ cation coordinated polymer matrix into dodecyl amine (DDA) modified montmorillonite clay (DMMT) galleries having a channel width of ∼16 Å. Structural, microstructural, stability (thermal, voltage), electrical conductivity (before and after polymer phase transition) and ion transport properties are analyzed.

2. Materials and methods

2.1. Sample preparation

Free-standing polymer clay nanocomposite (PNCE) films were prepared using high purity (AR grade) poly(ethylene oxide) (PEO) from Aldrich (USA), salt ($LiClO_4$) from (M/s Acros Organics) and Na-montmorillonite (MMT) (SWy-2) supplied by the Clay Minerals Society (USA). The MMT is organically modified using dodecylamine as a surfactant by an ion-exchange reaction. In the process, Na^+ ions, the natural occupants of clay channels, are replaced by dodecyl ammonium ion and hence the MMT becomes organophilic. As a result, the ambiguity of the presence of the two alkali cations (Li^+ and Na^+) of the PNCE films in the clay channel is resolved. The process for organo-modification of clay was followed from literature [20]. PCNE films were prepared by a solution-casting technique with different weight ratios of modified montmorillonite clay. The precursors were vacuum dried and the host polymer (PEO) and salt ($LiClO_4$) were dissolved in acetonitrile at a constant ratio of ether oxygen to lithium ion (O/Li) ∼8:1. The polymer–salt solution was stirred for 8 h followed by the addition of modified montmorillonite (MMT) clay. Subsequently, this viscous composite fluid was cast into a polypropylene dish and the solvent was allowed to evaporate slowly. The resulting free-standing clay based polymer nanocomposite (PNCE) films have the general formula: ($(PEO)_8LiClO_4$ + *x*wt.% DMMT) where *x* varies from 0 (pure polymer–salt complex, PS) to 20 wt.% with respect to the host polymer (w/w).

2.2. Sample analysis

X-ray powder diffraction (XRD) patterns of the PNCEs were taken using Rigaku Miniflex X-ray diffractometer with Cu Kα radiation (λ = 1.5405 Å). Sample microstructure was studied by transmission electron microscopy (TEM) analysis using C M 12 PHILIPS TEM equipment. Samples for TEM analysis were prepared by a drop casting-technique on a carbon coated copper grid. The samples were dried for 24 h in vacuum prior to scanning under the transmission electron microscope. The distribution of clay particulates in the PS matrix was examined by an energy dispersive X-ray (EDAX) dot mapping technique available in the scanning electron microscope (SEM JOEL-JSM Model 5800). Thermal analysis techniques of differential scanning calorimetry (DSC) and thermo-gravimetric analysis (TGA) were carried out using PerkinElmer (Model: Sapphire DSC)

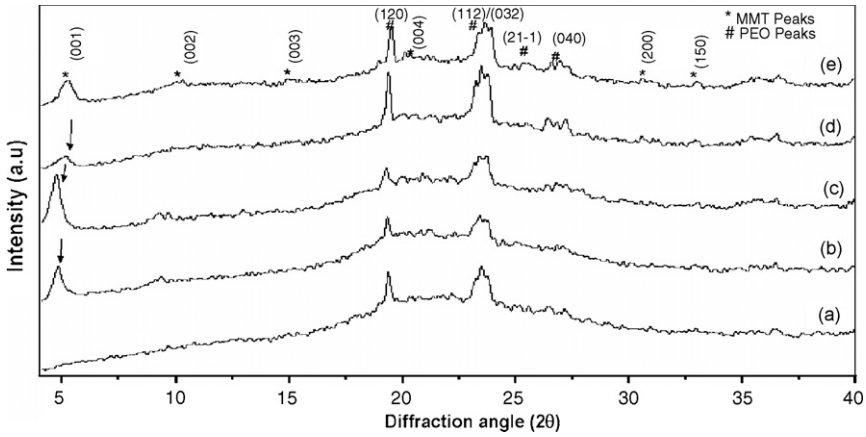

Fig. 1. X-ray diffraction pattern of PEO_8LiClO_4 + *x*wt.% DMMT based polymer nanocomposite (PNCE) films: (a) *x* = 0, (b) *x* = 2, (c) *x* = 5, (d) *x* = 15, (e) *x* = 20.

and (Model: Diamond TG/DTA) set-ups, respectively. Nanocomposite film samples of weight ∼10–15 mg were hermitically sealed in standard aluminum pans prior to experiment and put in the DSC chamber. Thermograms were recorded at a scan rate of 10 °C per min in an argon atmosphere with a flow rate of 50 ml per min in the temperature range of −90 to 150 °C for DSC and 200 ml per min for TGA measurements up to a temperature of 500 °C starting from room temperature. The electrical conductivity (dc) of the PNCE films was determined with a two probe ac technique of complex impedance spectroscopy with a HIOKI LCR Hi-Tester (Model 3532, Japan) in the frequency range of 100 Hz to 1 MHz. The film samples were placed in a symmetrical cell configuration of SS|PNCE|SS (SS stands for stainless-steel blocking electrodes and PNCE for the polymer nanocomposite electrolyte). An ac input signal of 20 mV (peak to peak) was applied across the cell for recording the impedance spectra of the films over a range of temperature. The experimental impedance data were subjected to non-linear least squares fitting using a ZSimWin-2.00 program. The electrochemical stability (i.e., working voltage) of the PNCE films was measured from the variation of residual electronic current as a function of the applied voltage across the test cell. The resulting *I*–*V* characteristics gave an estimate of the "optimum working voltage" limit estimated in terms of the point of intercept of the suddenly rising current on the voltage axis. The ion transport numbers of the sample materials were determined by measuring the polarization current as a function of time across the given material sample inserted between two blocking electrodes at a constant applied dc voltage ∼50 mV. The experimental values of the total current (I_T) on immediate voltage application and the saturated electronic current (I_e) give an estimate of the ionic and electronic transport numbers in accordance with the relation;

$$t_{ion} = \frac{I_T - I_e}{I_T}, \quad \text{where } I_{ion} + I_e = I_T \text{ and } t_{ion} + t_e = 1 \tag{1}$$

3. Results and discussion

3.1. Structural analysis

The X-ray diffraction (XRD) patterns of polymer nanocomposite films based on the stoichiometric combination PEO_8LiClO_4 + *x*wt.% DMMT are shown in Fig. 1. The characteristic features of the diffraction patterns are: (i) the presence of a broad background hump for clay free PS film, (ii) the typical signature of the crystalline phase of PEO major peaks appearing at ∼19.5 and ∼23.5° followed by low intensity diffraction peaks at 26.3° and 27° and (iii) diffraction peaks of the PS and DMMT clay based polymer nanocomposite (PNCE) films appearing as independent entities. These observations confirm composite formation and multiphase characteristics of the PNCE films that are comprised of amorphous and crystalline components. Distinct changes appear in the XRD pattern upon addition of clay to the PS matrix. The diffraction peaks of the PEO–salt complex are indexed as (1 2 0), (1 1 2)/(0 3 2), 2 1 $\bar{1}$ and (0 4 0) at 19.2°, 23.4°, 26.3° and 27° respectively. The indexing sequence suggests that the PEO–$LiClO_4$ (PS) matrix still has the helical structure inherited from the parent polymer [21,22]. However, the helical structure may have become distorted to some extent in order to accommodate the lithium ion within its backbone on complexation. Further, polymer–salt complexation causes a small shift in peak position for both the main PEO peaks (at 19.5°, 23.5°). The profile of these peaks changes significantly on composite formation with clay. In order to observe the effect of clay loading on PS crystal structure, the main PEO peaks (at ∼19.5° and ∼23.5°) are analyzed separately (Fig. 2). The XRD spectra show that PEO peaks shift to the higher angle side and thereby indicate a definite effect of clay on the crystalline phase of PS film. The changes in the crystallite size of the semicrystalline of the PS matrix on nanocomposite formation are listed in Table 1 though there is not any major change in terms of the *d*-spacing of PS peaks.

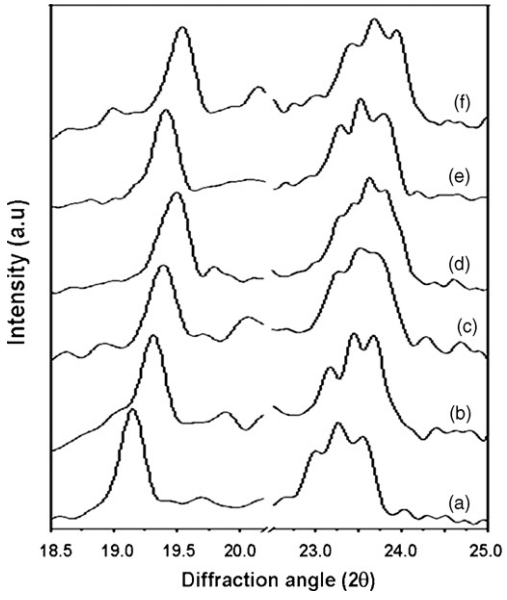

Fig. 2. XRD pattern of PEO main peaks of PEO_8LiClO_4 + *x*wt.% DMMT based polymer nanocomposite films: (a) *x* = 0, (b) *x* = 2, (c) *x* = 5, (d) *x* = 7.5, (e) *x* = 5, (f) *x* = 20.

Table 1
Effect of clay on changes in profile of PEO main XRD peak [(1 1 2), (0 3 2)] at $2\theta \sim 23^\circ$ for PEO_8LiClO_4 + *x*wt.% DMMT.

Clay concentration (*x*wt.%)	$2\theta = 23^\circ$				
	d-Spacing (Å)	Change in intensity ratio (I_{comp}/I_{PS})[a]	FWHM (rad × 10^3)	Crystallite size (l_c) (nm)	Change in l_c (%)
0	3.78	100	11.6	16.9	100
1	3.77	78.4	13.2	14.4	85
2	3.79	95.8	12.9	15.9	94
5	3.74	87.4	13.0	13.6	80
7.5	3.77	122.1	13.5	13.9	82
15	3.79	108.0	12.9	15.6	92
20	3.76	87.9	13.2	13.9	82

[a] I_{PS} and I_{comp} are the peak intensities for clay free PEO_8LiClO_4 complex and nanocomposites, respectively.

It appears from the XRD data presented in Table 1 that the changes in the PEO peaks observed in terms of peak shift, intensity variation and general profile tunability with changing clay concentration (Fig. 2) are significant. On immediate clay addition (say 1 wt.%) substantial lowering of the peak intensity ($I_{comp}/I_{PS} \sim 78\%$) and appreciable increase in full width at half maximum (FWHM ~ 14%) provide unambiguous evidence of a strong interaction of clay with the host polymer in the polymer nanocomposite (PNCE) film. Further, Table 1 also presents a comparative values of the interplanner spacing (*d*-spacing) and Scherrer length (l_c) calculated for the most intense PEO peak. There is an initial peak shift towards a higher angle side for $x \leq 10$ wt.% clay beyond which PEO peaks again show backward shift on the diffraction angle (2θ) scale for $x > 10$ wt.%, whereas the *d*-spacing remains almost unaffected by changes in clay concentration. On the other hand, a comparison of the Scherrer length (l_c) of PEO for different clay concentrations indicates that the crystallite size of the PEO has been affected significantly in the PNCE films. This is also corroborated by a lowering in the intensity of the [(1 1 2)/(0 3 2)] peak of PEO in the PNCE films relative to the PS film intensity (expressed in terms of the ratio I_{comp}/I_{PS} in Table 1). Such a lowering in the intensity accompanied by an enhancement in the FWHM in the PNCE films suggests suppression of the crystalline component of the polymer host (PEO) on clay addition due to a strong interaction between the PS–clay components. This possibility appears to be consistent with a previous report [8] that the crystallinity of the host polymer in a polymer–clay nanocomposite decreases on intercalation of PS in the clay channels (galleries) of nanometer dimension. PS intercalation also results in a lowering of its density inside the clay galleries. However, this result does not indicate whether PS intercalation into the clay is partial or complete. In contrast to this observation, a published study [23] of melt intercalated PNCEs claimed that full intercalation occurs at a critical polymer:clay ratio of ~28:72. [23]. Such a PNCE basically represents clay as matrix with significant loss of dimensional stability and the advantage of using a polymer. In order to obtain convincing evidence of PS intercalation into the clay galleries, we have carried out a systematic analysis of the changes in the clay peak profiles of the PNCE films.

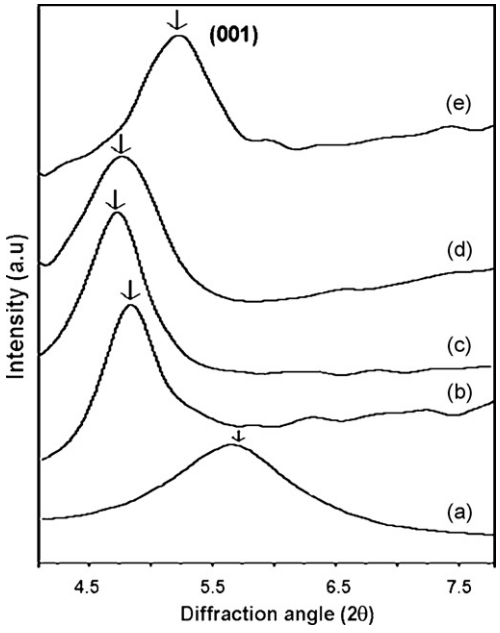

Fig. 3. Changes in d_{001} (basal spacing) of clay peak in PNCE films for (a) organo modified montmorillonite, (b) $x = 2\%$ (c) $x = 5\%$, (d) $x = 10\%$ and (e) $x = 20\%$ of montmorillonite in PEO_8LiClO_4 + *x*wt.% DMMT.

The feasibility of PS intercalation in clay galleries has to be investigated with reference to the basic crystal structure of the inorganic clay and changes occurring therein on modification, if any. The Na-montmorillonite clay used in the present studies, in its naturally occurring form, has a triclinic crystal structure with the crystal axes '*a*' and '*b*' being continuous such that they stack one upon another in '*c*'-direction forming layers. The layers are comprised of edge-sharing octahedral sheets of aluminium hydroxide flanked by a tetrahedral silicate sheet on either side. The space between the edge-shared octahedral and tetrahedral silicate sheets of the clay, which has a width of nanometer size, gives rise to the nanometric clay channel/gallery. The width can be estimated from the XRD data in accordance with the relation: $W_{cg} = d_{001} - W_{cl}$, where W_{cg} = width of the clay channel (gallery), d_{001} = basal spacing in *c* direction, W_{cl} = clay layer width in *c*-axis.

In an unmodified clay, $W_{cl} = 9.6$ Å [9], and $d_{001} = 12.0$ Å so that the width of the clay gallery (channel) is such that (W_{cg}) = 2.4 Å. This width is occupied mostly by hydrated cations in the natural clay, which are exchangeable. On modification of this natural clay by dodecyl amine (DDA) under controlled conditions, the hydrophilic cations are exchanged by dodecyl ammonium ion and result in an increase in gallery width to 6 Å from its initial value of 2.4 Å (Table 2). Information on such changes occurring in the clay layers has been obtained by profile analysis of the most intense XRD peak of the clay that occurs at $2\theta = 5^\circ$ and is attributed to d_{hkl} = (0 0 1) [24]. Substantial changes in the d_{001} peak profile of the organo-modified montmorillonite (DMMT) clay in the PNCE film are observed when compared with that of pure clay, as shown in Fig. 3. The changes are evident in terms of a peak shift towards the lower angle side, an increase in *d*-spacing, an increase in peak intensity and an enhancement in the clay gallery width in the PNCE film when compared with pure clay peak data for these parameters (Table 2). The appearance of a peak shift towards the low angle side and an appreciable increase in the basal plane spacing (d_{001}) of the clay occurs immediately on clay addition (~1–2 wt.%) to the PS matrix. Further, the clay channel (gallery) width (W_{cg}) has also been found to increase by ~46% on the addition of an even small amount (~2 wt.%) of clay to the PS matrix. A comparison indicates that this width (W_{cg}) increases by ~53% with increase in clay of up

Table 2
Basal spacing, gallery width and Scherrer length in the (0 0 1) direction of MMT clay.

Clay concentration (*x*wt.%)	Peak position ($2\theta^{\circ}$)	*d*-Spacing (Å)	Clay gallery width (Å)	Peak width × 10^3 (rad)	Crystallite size (nm)
Unmodified MMT	7.3	12	2.4	28.0	5.0
Mod. MMT	5.6	15.7	6.0	17.2	8.0
2	4.8	18.3	8.7	6.2	22.3
5	4.7	18.6	9.0	8.3	16.5
10	4.7	18.6	9.0	9.4	14.6
15	5.1	17.3	7.7	9.1	15.2
20	5.1	17.5	8.0	10.4	13.2

to ∼10 wt.% in the PNCE film. For a clay concentration (x) > 10 wt.%, a relative decrease in the clay gallery width (W_{cg}) occurs with minimum value of 32% at 20 wt.% clay in the PNCE film.

The above findings from the clay XRD patterns of the PNCE films provide reasonable and convincing evidence of a very strong interaction of the PS with the clay matrix that is possibly assisted by dipolar interaction. Further, an increase in clay gallery width up to 9 Å in the PNCE films is in sharp contrast with that of the DMMT clay width ∼6 Å (Table 2) and confirms the possibility of intercalation (Fig. 3) of the PS matrix into clay channels of nanometer dimension. This conclusion seems to be logical and consistent with the fact that the PEO–$LiClO_4$ complex (PS) has a helical structure with a tunnel radius in the range of ∼(1.3–1.5) Å [25]. In view of the physical dimensions of the PS structure and clay channels, intercalation of either two layers of the helically structured PS or a monolayer of randomly oriented PS can be expected. The latter possibility has been predicted from theoretical considerations and also observed experimentally [16]. However, the possibilities discussed above based on XRD results require further confirmation and support by TEM analysis. Further, the observations from XRD analysis suggest that the PNCE films have a multiphase combination of crystalline and amorphous PS phases, an amorphous phase boundary, crystalline clay and amorphous PS inside the clay galleries at the interface of the clay layers and PS matrix.

3.2. Microstructural studies

It is well established from experimental results that MMT clay has channels/galleries of nanometer dimensions [5–8]. Transmission electron microscopy (TEM) analysis has been carried out to investigate the microstructural features of the PNCE films and also to observe the change in surface property/morphology on intercalation of PS into the nanometric clay channels. Representative TEM micrographs and selected area diffraction (SAED) patterns of PNCE films with varying clay concentration are given in Fig. 4a–f. The typical morphology of the clay-free PS matrix (Fig. 4a) exhibits its multiphase character that is comprised of crystalline and amorphous components. This observation is corroborated by the SEAD pattern of the PS sample that shows well-defined rings at the centre followed by hollow region thereafter (Fig. 4b). The surface morphology of the clay dispersed films changes drastically as revealed by TEM micrographs (Fig. 4c and e) and the corresponding SAED patterns (Fig. 4d and f) for 5 and 20 wt.% clay reinforcement in the PS film. It is believed that the degree of dispersion of the clay particulates into the PS matrix controls the structure and morphological features of the composite nanostructures. The dispersion depends on the nature and strength of the interaction between the PS and clay components in the PNCE films. TEM results in the present study provide direct evidence of the clay concentration dependant interaction among the components (PS and clay) in the PNCE films. At a low concentration of clay (≤5 wt.%), the individual layered silicates appear to be dispersed randomly in the PS matrix to field an exfoliated structure in the nanocomposite. In addition to this feature, evidence of alignment of silicate layers (marked with arrow) for 5 wt.% clay sample (Fig. 4c) is also observed. The results suggest that, although exfoliation is likely at a low clay loading, the possibility of intercalation cannot be ruled out. The TEM micrographs for clay loadings ≤5 wt.%, together with the SAED pattern for the 5 wt.% clay film (Fig. 4c and d), provide convincing evidence for partially exfoliated and intercalated structures in PNCE films. This conclusion also appears to be well correlated with XRD analysis and is in accord with previous investigation [26,27].

As the clay concentration increases (≥7.5 wt.%), coherent stacking of silicate layers of nanometer dimensions occurs as shown in Fig. 4e. The dark lines are silicate layers of the organo-modified clay with which the PS matrix has been reinforced in the polymer nanocomposite film. The presence of the silicate layers, separated from each other by ∼1 nm in excellent agreement with the calculated values from XRD results, provides unambiguous evidence of an intercalated composite nanostructure. The origin of such nanostructure lies in the entry of a cation coordinated single polymer chain into the nanometric channels between the silicate layers.

The evidence of exfoliation/intercalation at low clay concentrations has prompted further investigation of the concentration profile of clay particulates in the PS matrix by means of a EDAX dot-mapping technique. Dot mapped micrographs depicting the distribution of the Si-atoms of the silicate clay are shown in Fig. 5a–d. The DMMT clay particulates are homogeneously distributed throughout the matrix without any sign of aggregation at low clay loadings up to 10 wt.% (Fig. 5a–c). At higher clay concentrations, however, though the distribution of clay particulates is still homogeneous, there is evidence of tiny clay clusters in 20 wt.% of clay, as demonstrated in Fig. 5d.

3.3. Thermal analysis

The differential scanning calorimetry (DSC) patterns of the PS and clay intercalated polymer nanocomposite (PNCE) films are shown in Fig. 6a–g. A comparison of the DSC thermograms for PS with those of PNCE films suggests substantial changes in thermal transitions and their profiles observed in terms of thermodynamic parameters of the system under study such as glass transition temperature (T_g), broadening width of T_g (ΔT_g), heat capacity change (ΔC_p), crystalline melting temperature (T_m), enthalpy change (ΔH_m), and fraction of crystalline content (X_c). A quantitative estimation of these parameters from DSC results has been made for the PNCE films of different clay concentrations and is recorded in Table 3. The DSC pattern of the PS film comprises of a step change in the sub-ambient temperature range owing to glass transition temperature occurring at $T_g \sim -39\,^{\circ}C$. Relative changes in the value of the PS glass transition temperature (T_g), estimated from the mid-point of the step change in the DSC thermogram, with clay concentration are given in Table 3. The data show a systematic decrease in the value of the T_g up to 5 wt.% clay and thereafter increases for 7.5 wt.% clay. In general, the T_g values for the PNCE films are mostly lower than those of PS. This may be attributed to improvement in the flexibility of the polymer host backbone assisted by intercalation on nanocomposite formation. Further, changes in T_g of the polymer host with clay concentration in the PNCE films also sug-

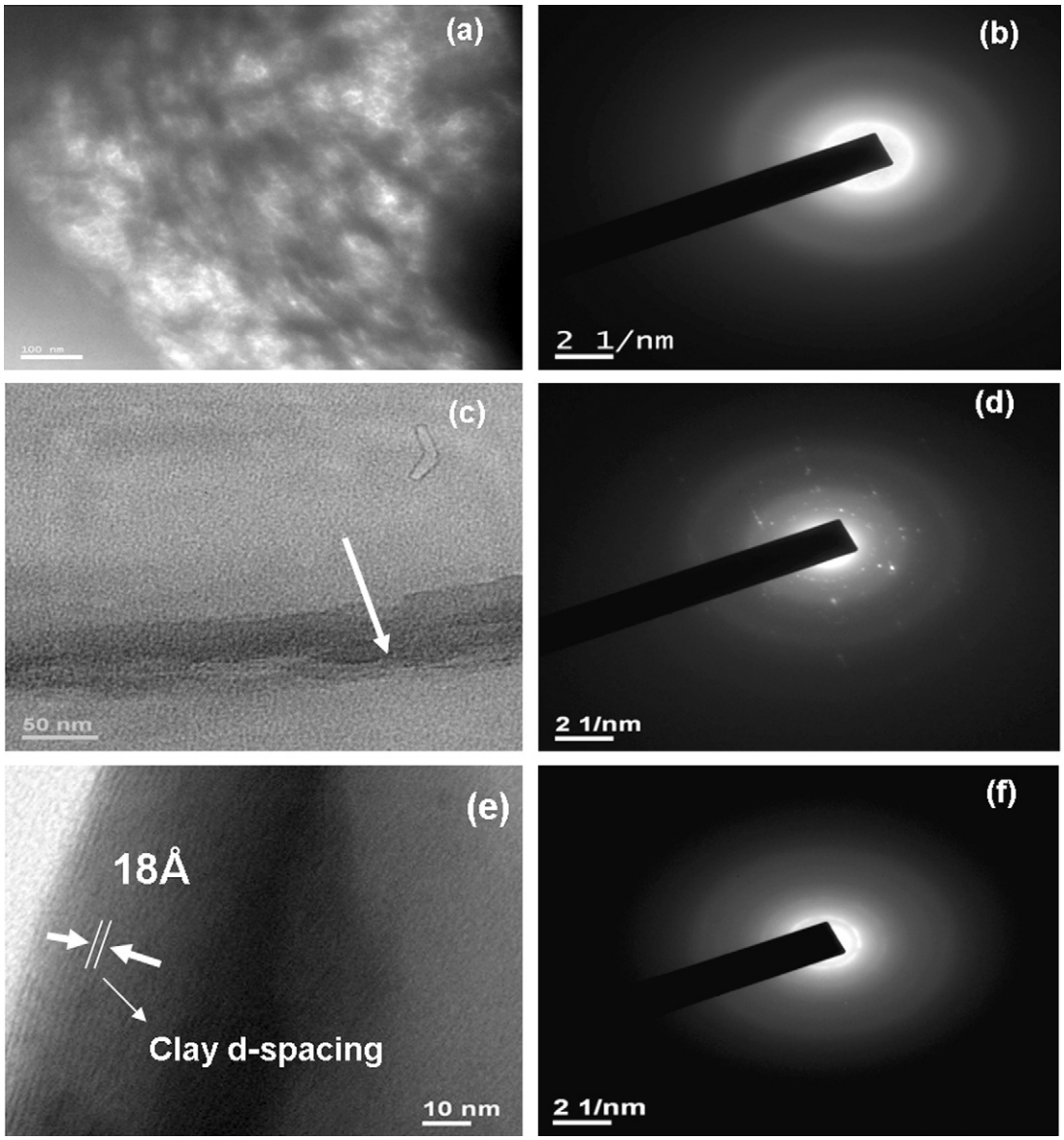

Fig. 4. TEM micrograph of PS, 5 wt.% and 20 wt.% DMMT dispersed PNCEs in (a), (c) and (e) respectively. Selective area electron diffraction (SAED) patterns are given sequentially in (b), (d) and (f) next to corresponding image patterns.

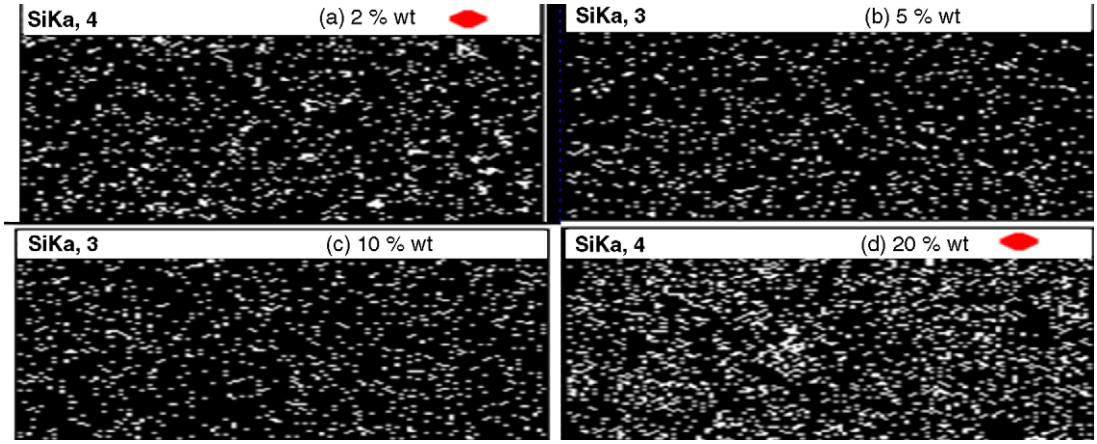

Fig. 5. EDAX dot mapping images (of Si atom in clay layers) for PNCEs showing concentration profile of montmorillonite clay particulates in PS matrix.

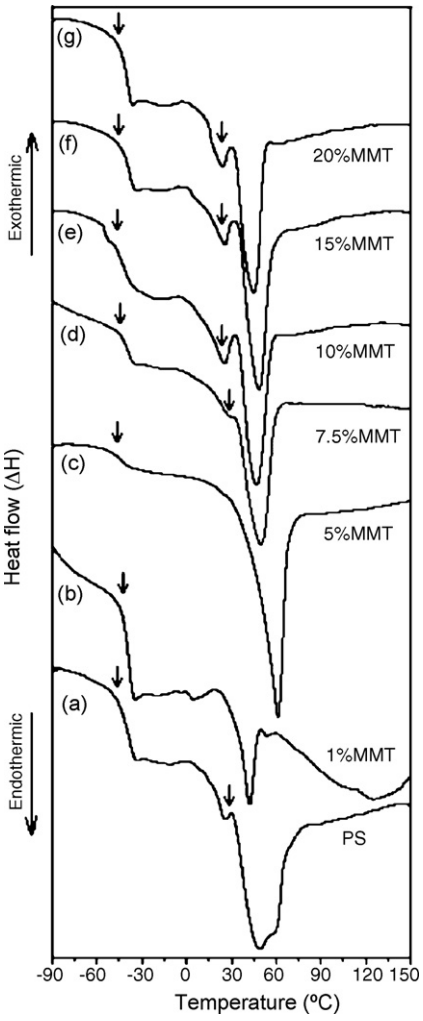

Fig. 6. Differential scanning calorimetry (DSC) plots of polymer nanocomposite films based on $(PEO)_8LiClO_4$ + *x*wt.%; DMMT clay for (a) $x = 0$, (b) $x = 1$, (c) $x = 5$, (d) $x = 7.5$, (e) $x = 10$, (f) $x = 15$, (g) $x = 20$.

gest a strong possibility of clay interaction with the PS component in the composite films.

It is believed that the glass transition temperature determines the extent of flexibility of the polymer network. So a lowering in the value in the PNCE films provides clear evidence of the polymer host phase transition from a rigid framework structure to a flexible elastomeric phase on nanocomposite formation. Thermodynamically, such a phase transformation is denoted as a second-order phase transformation. The strength of such a transition can thereafter be evaluated in terms of glass transition width (ΔT_g) and changes in the heat capacity (ΔC_p) of the PS film as a function of clay concentration. These parameters provide vital information on the type of thermal transition process occurring in the ionically conducting polymer–salt complex film and on the effect of clay concentration on intercalation nanocomposite formation. The observed values of ΔT_g and ΔC_p are given in Table 3 for different clay concentrations in the PNCE films. ΔT_g, which represents the difference between the onset and end-point of glass transition phenomena, is a direct indicator of the mechanism (number/type) of relaxation process occurring during glass transition. A relative increase in ΔT_g with increase in the clay concentration in the PNCE films indicates a broadening of the glass transition process on intercalation of PS into the clay channel in the PNCE films. In turn this broadening causes a lowering of T_g and a significant change in the relaxation mode of the polymer chain with increasing clay concentration in the PNCE films. The presence of thermally activated relaxation, indicated by ΔT_g broadening in the PNCE films that have a heterogeneous composition, appears to be logical in view of a number of possibilities such as: (i) dipole–dipole interaction due to the presence of free cations, a cation coordinated polymer, free anions, ion-pairs and dipolar clay; (ii) changes in the orientation of polymer chain with temperature in a matrix having Coulombic interaction; (iii) hydrogen bonding. Each of these individual contributions has its own characteristic relaxation time whose complex interaction ultimately results in broadening of the glass transition region. The highest value of $\Delta T_g \sim 22\,^\circ$C for PNCE films with 2–5 wt.% clay followed by $\Delta T_g \sim 21\,^\circ$C for 10 wt.% clay has been recorded. This indicates that there are two critical concentrations in the PNCE series of films where interaction among constituents favours a broadened glass transition that results in chain flexibility/relaxation. A quantitative estimation of this relaxation strength near the kinetic glass transition may be obtained in terms of the change in free volume of the system in the relevant temperature range. It is expressed in terms of caloric relaxation strength (ΔC_p) and the values are given in Table 3 for different clay concentrations in the PNCE films. It appears that the value of ΔC_p is, in general, lower for all composite films in comparison with that of a PS film with its minimum value for 2–5 wt.% of clay composition. This result suggests the possibility of a very strong interaction of the PS with clay surfactants on nanocomposite formation in good agreement with the results of XRD and TEM analyses in the present studies. This interaction causes a lowering of entropy, free energy and T_g as indicated by the discontinuous change in the sub-ambient region which according to:

$$-\frac{C_p}{T} = -\left(\frac{\partial S}{\partial T}\right)_P = \left(\frac{\partial^2 G}{\partial T^2}\right)_P \quad (2)$$

It is a characteristic feature of the second-order phase transition attributed to the host polymer where a non-linearity in ΔC_p relative to the clay concentration is indicative of a process with very strong interaction among the constituents of the nanocomposite system.

Table 3
Thermodynamical parameters calculated from DSC results of PEO_8LiClO_4 + *x*wt.% DMMT based nanocomposite films.

Clay loading (wt.%)	Glass transition parameters			Crystalline melting point (T_m) (°C)	Enthalpy (J g^{-1}) normalized	PEO crystallinity (%X_c)
	Glass Transition T_g (°C)	Width of T_g (ΔT_g) (°C)	ΔC_p (J g^{-1} °C^{-1})			
0	−39	16	0.69	48.4	42.2	29.1
1	−40	16	0.55	–	–	–
2	−40	22	0.13	55.3	20.8	14.5
5	−44	22	0.19	61.2	80.4	57.5
7.5	−39	18	0.36	49.5	41.1	30.0
10	−44	21	0.41	46.6	28.7	21.3
15	−39	19	0.54	48.2	35.6	27.4
20	−40	21	0.50	44.6	25.1	20.0

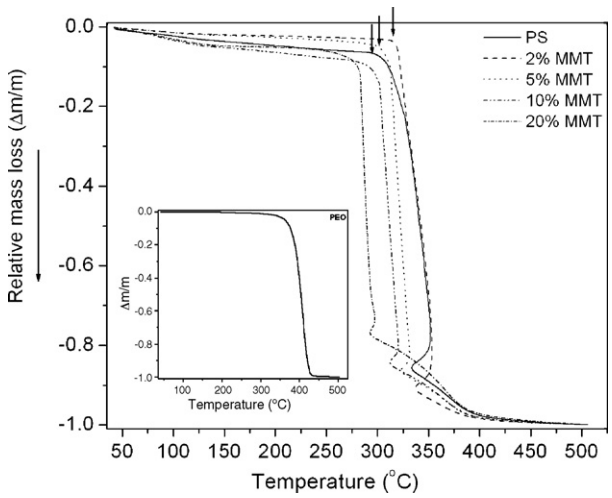

Fig. 7. Thermogravimetry analysis (TGA) plots of polymer–salt complex (PS) and polymer based nanocomposite (PNCE) films having different clay concentration compared with TGA pattern of pure PEO (inset).

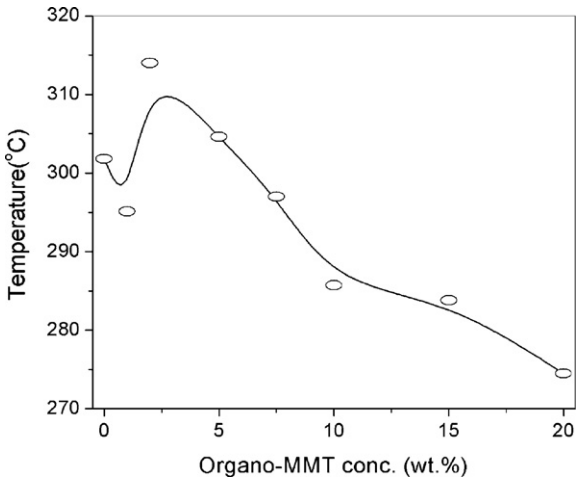

Fig. 8. Variation of degradation temperature (T_d) as function of DMMT clay weight fraction.

The DSC thermogram of the PNCE film in the temperature range $0\,^{\circ}C < T \leq 60\,^{\circ}C$ is comprised of endotherms observed at ~30 and 50 °C which are followed by a broad region in the temperature range 90–120 °C. The latter effect is a predominant feature in the PNCE sample with 1 wt.% clay concentration. The endotherms observed at 30 °C have been attributed to dehydration of residual acetonitrile solvent used in the sample preparation whereas the predominant endotherms observed in the temperature range 48–61 °C are assigned to the crystalline melting of uncomplexed PEO. The second endotherm is a characteristic feature in such multi-phase PNCE films and suggests the presence of an uncomplexed PEO component having uncoordinated ether oxygen in the host matrix. The area of this endotherm gives an estimate of the net heat flow (enthalpy) during structural phase transformation of PEO under the influence of temperature. This phase transformation is essentially of the first-order type and the net heat flow during the process gives an estimate of the change in crystallinity of the host PEO on composite formation. These parameters, as evaluated from DSC data, are given in Table 3.

Thermogravimetric analysis (TGA) results indicate a distinct change in the mass of the PNCE films relative to their initial mass (Fig. 7). The TGA patterns of PS and PNCE indicate that each can be divided into four regions: (i) a very slowly varying flat region from 50 to 300 °C; (ii) a sharply falling region (300–350 °C) that provides a signal for thermal degradation; (iii) a steadily decreasing mass loss region after a kink (300–400 °C); (iv) a flat region above 400 °C. The thermal stability has been estimated in terms of the degradation temperature (T_d) values observed from the TGA data. A comparison of the T_d of PS and PNCEs with that of pure PEO (Fig. 7, inset) indicates that the thermal stability of PS is certainly lower than that of PEO. However, the loss of stability in the PS matrix gets adequately compensated on nanocomposite formation with lower clay content (2–5 wt.%). In fact, thermal stability is significantly improved on intercalation when a cation coordinated polymer chain enters into the clay galleries. The variation of T_d with respect to clay concentration, shown in Fig. 8, clearly suggests that thermal stability improves on nanocomposite formation up to 5 wt.% of clay. Beyond this, thermal stability decreases monotonously for higher clay concentrations (>5 wt.%). It is noted that T_d has a value of 314 and 305 °C for 2 and 5 wt.% clay loaded PNCE films respectively. This is in sharp contrast to the $T_d \sim 302\,^{\circ}C$ of PS. In view of the experimental results observed in the present studies, it appears very difficult to generalize that the stacking of polymer chains into clay galleries will offer protection from thermal degradation. On the contrary, it can be presumed that the thermal stability in the PNCE films depends on two competing processes [28,29]: (i) *a barrier effect*—the clay layers may be acting as a barrier for decomposition of PS inside the clay galleries; (ii) *a catalytic effect*—such that the clay sheets act as a thermal reservoir and cause an accumulation of heat. This effect may be expected to accelerate PS decomposition and result in a lowering of the degradation temperature (thermal stability). The second possibility seems to be more effective with increase in clay concentration in the PNCE. As a consequence, the degradation temperatures of PNCE films for clay loadings >5 wt.% are lower than that of PS. This inference is logical based on experimental evidence and is consistent with reports in the literature [30–32].

Further, the appearance of a kink during the decomposition process is observed for PS and PNCE, invariably for the whole range of clay concentration under investigation. Such a kink is not present in pure PEO (inset). A comparison of this feature in PEO and PS indicates that the origin of the kink lies in the polymer–salt complexation process. On clay addition, the kink exhibits a relative change in its profile in the PNCE films according to the clay loading. This result is a specific one in the present investigation and can be used to estimate the fraction of uncomplexed polymer in the PS and PNCE films by comparing the changes in the kink profile for sample films with of different clay reinforcements. The estimated value shows that PS has a 15 wt.% uncomplexed PEO fraction whose value in the PNCE films varies with clay concentration. Composites with better thermal stability have lower amounts of uncomplexed PEO. The results indicate that composites with lower clay concentration (1–5 wt.%) have 10–15 wt.% pure PEO, whereas the value from 20 to 25 wt.% for composites with higher clay content. A relative decrease in the uncomplexed PEO fraction in the PNCE films with low clay content may be related to a higher degree of cation coordination assisted by strong interaction of the PS matrix with the clay layers. On the other hand, increase in the fraction of uncomplexed polymer at higher clay loadings (≥5 wt.%) may possibly be the result of enhanced ion-pair formation that reduces the number of cations available for coordination with the host polymer. This possibility appears to be feasible in view of the vibrational spectroscopy analysis reported elsewhere [33]. The inference also appears to be consistent and convincing based on previous reports in literature [2–4]. The overall impact of interaction of the PS matrix with clay is to effect a change in the dynamics of the polymer chain mobility that, in turn controls the electrical properties. This aspect is discussed in the next section.

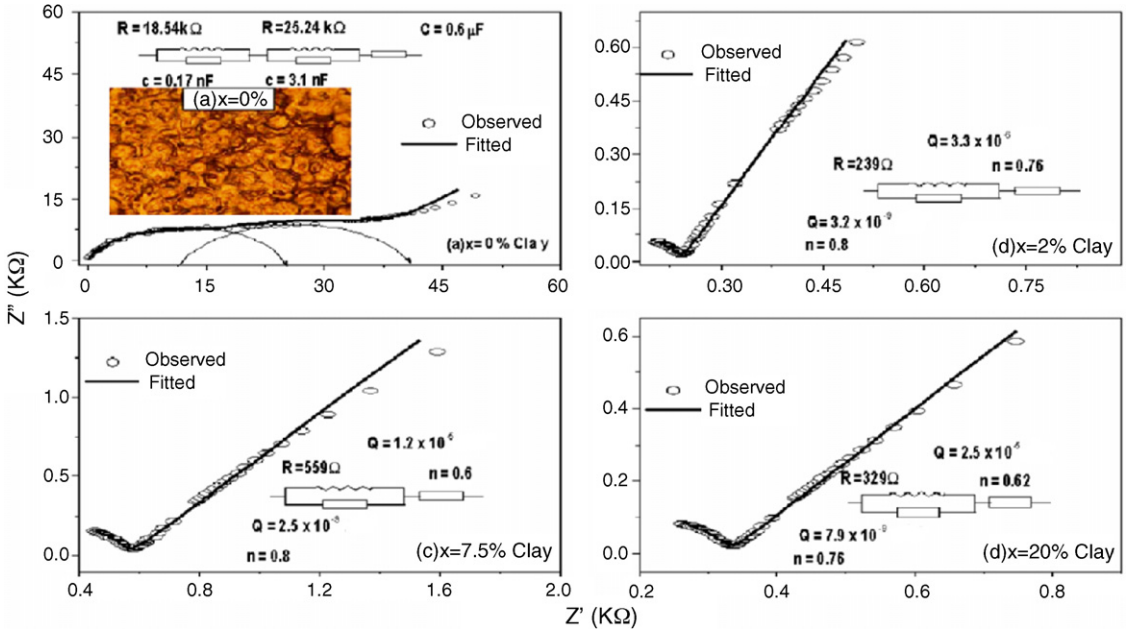

Fig. 9. Room temperature (30 °C) complex impedance (Z′–Z″) plot for PNCE films for different clay concentrations: (a) $x = 0$, (b) $x = 2$, (c) $x = 7.5$, (d) $x = 20$ wt.% and optical micrograph (inset) of polymer–salt complex showing spherulitic multiphase character.

3.4. Electrical analysis

The complex impedance spectra (CIS) of PS and clay-based nanocomposite films at room temperature are shown in Fig. 9. The CIS pattern of the PS film consists of a high-frequency semicircular arc followed by another arc at an intermediate frequency and a small spike evolving at the lower end of the frequency spectrum. The high frequency arc is attributed to contributions due to the bulk sample whereas the second semicircular arc can be related to the presence of a phase boundary effect that is predominantly due to the semicrystalline microstructure as revealed in its optical micrographs shown in the inset of Fig. 9a [34]. The presence of a spike in the low-frequency region suggests the formation of a space-charge layer, commonly referred to as the double-layer capacitive effect, due to a non-Faradaic process occurring at the polymer film|electrode interface [35]. The presence of two semicircles followed by a weak spike suggests that the PS film is electrically equivalent to a series combination of two parallel cascading of resistors (R) and constant phase element (cpe) in conjunction with another cpe. The term 'cpe' is more often used in place of capacitance in impedance fittings where material behaviour is different from that of a pure capacitor characterized by marked depression in the ideal semicircular pattern. The impedance associated with 'cpe' is expressed as: $Z_{cpe} = Y_o^{-1}(j\omega)^{-n}$, where $j = \sqrt{-1}$, and Y_o and n are the fitting parameters. Resistance, Warburg impedance, capacitance and inductance are examples of cpe for $n = 0$, 0.5, 1, and -1, respectively [36]. The dimension of cpe is $\Omega^{-1}\,s^n$ whereas that of capacitance is $\Omega^{-1}\,s$.

On the addition of clay, the CIS pattern shows a drastic change. In the high-frequency region, there is only one semicircular arc followed by a spike in the low-frequency region of the dispersion pattern. Such a modification in the impedance spectrum of the nanocomposite films suggests a drastic change in the electrical properties of the PS film on intercalation in the clay matrix. The electrical properties now appear to be mainly due to the bulk contribution, possibly from intermingling of the phase boundary with the bulk matrix, such that the whole of the polymer matrix behaves as one component. The low-frequency response in the CIS pattern remains almost the same for the PNCE films as in the case of PS film irrespective of clay concentration. This behaviour results from the accumulation of space charge at the interface of the ionically conducting polymer film and stainless-steel blocking electrode.

The impedance spectra of PS and PNCE films of different clay concentrations have been fitted using the computer program ZSimpWin. The theoretical and experimental patterns appear to be in good agreement. The estimated values of the electrical parameters from the 'equivalent electrical circuit' are given in Fig. 9a–d, inset. From the values of R, Q and n, it appears that the clay concentration affects markedly the electrical properties of the PNCE films. The values also indicate that the cpe attributed to the bulk semicircle behaves more like a capacitor, whereas the cpe attributed to the spike exhibits a capacitive effect at low clay concentration and assumes near-Warburg type impedance characteristics at higher clay loadings in the PS matrix. This inference is also supported by an increase in interfacial capacitance by one order of magnitude in composites with a higher clay loading (i.e. 12 μF for 7.5 wt.% DMMT and 25 μF for 20 wt.% DMMT) than PS and PNCE with a low clay content (0.6 μF for PS and 3.3 μF for 2 wt.% DMMT). The intercept of the high-frequency semicircular arc with the real axis gives an estimate of the bulk (dc) resistance (R_b) and its value for the PS film is ~18.5 kΩ at room temperature ($T = 30$ °C). On the other hand, the bulk resistance value of composites has been estimated to be reduced by two orders of magnitude. The bulk and interfacial capacitive components for different clay loadings estimated from CIS results (Fig. 9) are in the order of nF and μF, respectively.

The CIS pattern of the PNCE film at 70 °C (above crystalline melting temperature, T_m) is shown in Fig. 10a–d. The impedance pattern at this temperature has the typical feature of a very small arc in the high-frequency region followed by a steep spike in both the PS and PNCE films, irrespective of their composition. The equivalent electrical circuit used to fit the impedance plot with software ZSimWin is given in the insets of Fig. 10a–d. It comprises of a parallel combination of resistance with capacitance arising from the bulk contribution to impedance response. The values of the R and C components are drastically reduced and this may be correlated with a lowering of the barrier to the mobility of charge carriers on the crystalline to amorphous phase transition of the host polymer. The reduced value of bulk resistance is followed by an enhanced

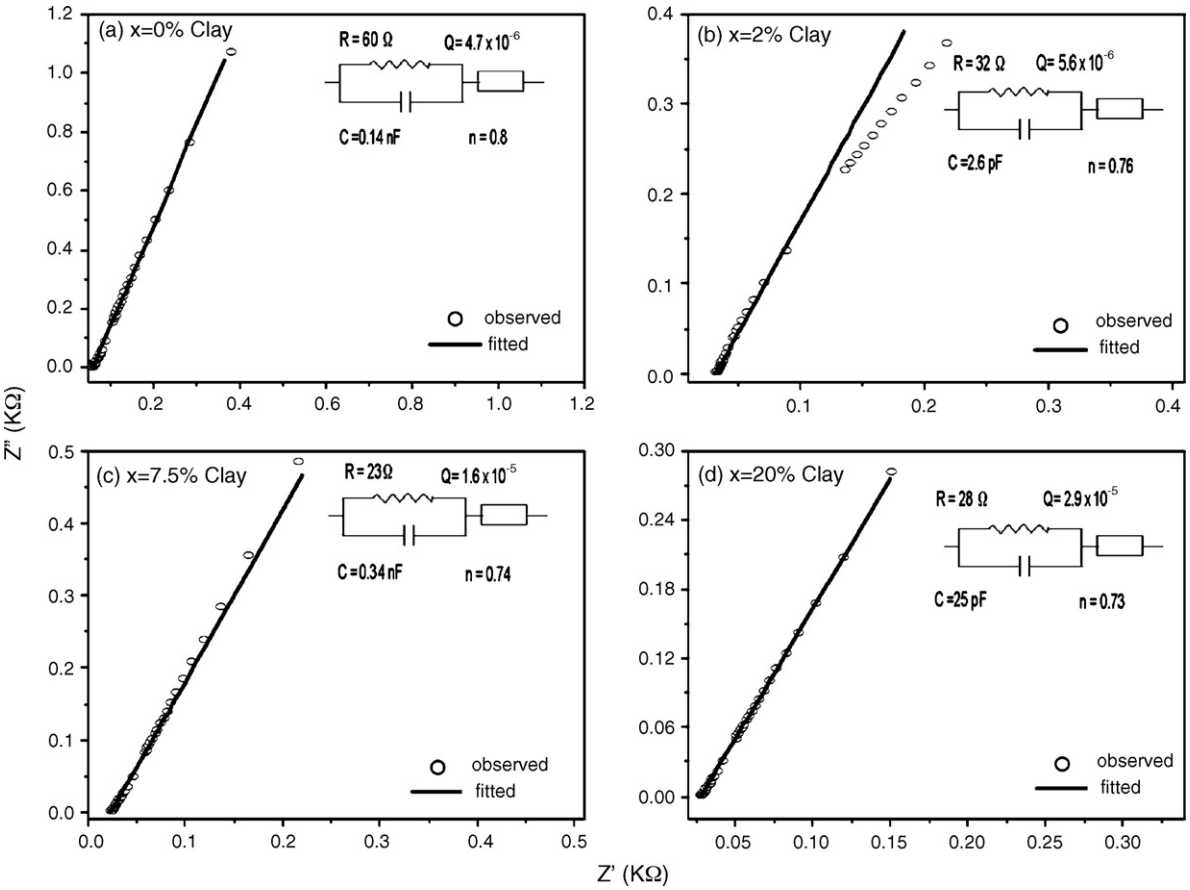

Fig. 10. Complex impedance (Z'–Z'') plot for PNCE films for different clay concentration: (a) $x = 0$, (b) $x = 2$, (c) $x = 7.5$, (d) $x = 20$ wt.% at 70 °C (above crystalline melting point).

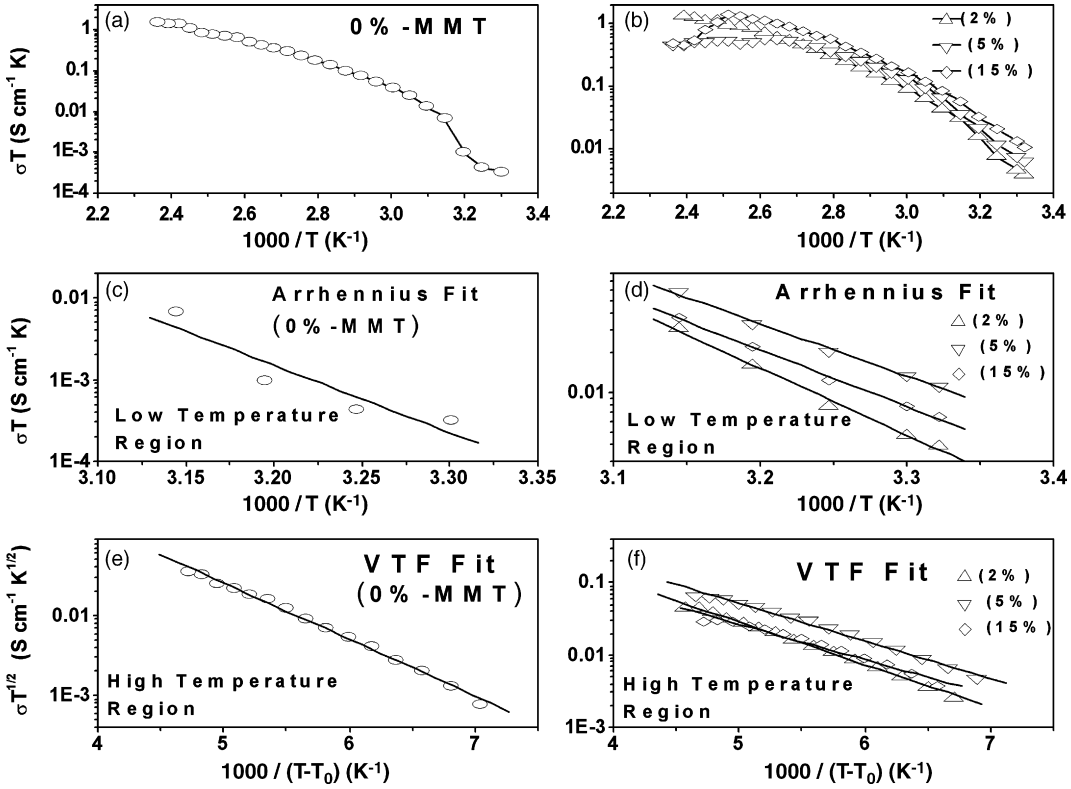

Fig. 11. Variation of dc conductivity of PS and PNCEs with $10^3/T$: (a) and (b) showing variation of σT vs. $10^3/T$, (c) and (d) shows the fitting of σT vs. $10^3/T$ below T_m with Arrhenius relation, (e) and (f) shows fitting of σT vs. $10^3/T - T_o$ below T_m with VTF relation. T_o is fitting temperature and is equal to $T_g - 50$ K. T_g is estimated from DSC analysis.

Table 4
dc conductivity parameters (activation energy and pre-exponential factor) in the Arrhenius region (below crystalline melting point; T_m) and VTF region (beyond T_m).

DMMT clay content (wt.%)	Polymer matrix crystallinity (%) (X_c)	dc conductivity (σ_{dc}) (S cm^{-1})					
		Before crystalline melting			After crystalline melting		
		30 °C	ln(σ_0 S^{-1} cm K^{-1})	Arrhenius E_a (eV)	70 °C	ln(σ_0 S^{-1} cm K$^{-0.5}$)	VTF E_a (eV)
0	29	4.44×10^{-7}	31.18	1.78	2.19×10^{-4}	4.44	0.14
1	...	9.16×10^{-5}	27.00	0.81	9.43×10^{-4}	2.86	0.10
2	15	6.12×10^{-5}	33.23	1.01	4.66×10^{-4}	3.34	0.12
5	57	3.27×10^{-5}	29.27	0.89	6.16×10^{-4}	2.35	0.10
7.5	30	3.11×10^{-5}	33.32	1.01	7.99×10^{-4}	3.90	0.12
10	21	6.48×10^{-5}	45.50	1.38	2.28×10^{-4}	2.63	0.12
15	27	3.73×10^{-5}	25.84	0.79	8.21×10^{-4}	3.45	0.11
20	20	5.59×10^{-5}	30.00	0.91	6.63×10^{-4}	3.06	0.11

interfacial polarization effect indicated by the cpe element in the equivalent circuit and is attributed to the appearance of a steep spike at high temperature due to accumulation of space charge at the interface. The interfacial capacitive components of PS and PNCE at low clay contents (2–5 wt.%) are of the same order at 70 °C. On the other hand, a comparison of the interfacial capacitance of PS at room temperature (0.6 μF for PS) with that at 70 °C (4.7 μF) indicates a major change in the double-layer interfacial capacitance value for PS. This large (~8 times) enhancement at high temperature can be attributed to increased charge accumulation at the interface assisted by faster ion (charge) transport in the PS film at $T \geq T_m$. An almost identical observation has been made for clay loaded PNCE films.

The variation of dc conductivity (σ_{dc}) from room temperature to 150 °C is shown in Fig. 11a–f. A semi-logarithmic plot of σT vs. $10^3/T$ for PS (Fig. 11a) and for PNCEs (Fig. 11b) shows a typical linear change in conductivity at low temperature followed by marked non-linearity with increase in temperature at and above ~65 °C. This transition in behaviour is observed for almost all the compositions and can be correlated to the structural phase transition (crystalline → amorphous) of the host polymer (PEO) that assists in liquid-like ion transport despite being solid in physical form. The conductivity pattern at low temperature exhibits typical Arrhenius behaviour, i.e.,

$$\sigma = \sigma_o \exp\left(\frac{-E_a}{k_B T}\right) \quad (3)$$

This indicates a thermally activated charge transport process that occurs via hopping of ions from one preferred site to another. The non-linear conductivity bhaviour at higher temperatures ($T \geq T_m$), at which the polymer matrix becomes predominantly amorphous with minimum internal friction (resistance) within the sample matrix, can be explained by the Vogel–Tamman–Fulcher (VTF) model of charge transport expressed by the relation;

$$\sigma = \sigma_0 T^{-1/2} \exp\frac{-E_a}{k_\beta [T - T_0]} \quad (4)$$

where σ_0 is a pre-exponential factor, k_β is the Boltzman constant, E_a is the activation energy, T_o is a fitting parameter called the reference temperature and is also identified as the glass transition temperature (T_g) of the polymer host above which the polymer backbone becomes flexible and permits motion of the polymer segment/chain in the matrix. The VTF model proposes that the ionic mobility at high temperatures ($T \geq T_m$) is favoured as a result of cooperative segmental motion of the polymer chain in the matrix. A linear fit of the temperature dependent conductivity data of the PS and PNCE films, fitted separately in the temperature range below and above polymer host T_m, is shown in Fig. 11c–f. The results agree well with the Arrhenius and VTF relations (Eqs. (3) and (4)) for $T \leq T_m$ and $T \geq T_m$, respectively. Conductivity data and other related parameters (activation energy and pre-exponential factors) estimated from the linear fits for each composite film are given in Table 4. The room-temperature conductivity shows a jump by two orders of magnitude (~208 times) from 4.44×10^{-7} S cm^{-1} for PS to 9.16×10^{-5} S cm^{-1} for the PNCE film even for a low clay loading (1 wt.%). There is a strong dependence of the conductivity of PNCE films on clay concentration. On the other hand, the conductivity of PNCE and PS is in the same range of ~10^{-4} S cm^{-1} at ~70 °C. The highest conductivity achieved is ~9.43×10^{-4} S cm^{-1} for a 1 wt.% clay-loaded PNCE film. The activation energy for PS before and after T_m is the highest, whereas its value is relatively lower in PNCE films though there is a concentration dependent variation. The mean activation energy in the VTF region is ~0.1 eV, which is one order of magnitude less than that in the Arrhenius region ~1.0 eV. These observations suggest a thermally activated hopping type mechanism of conductivity in the low temperature region ($T \leq T_m$). In contrast, electrical conduction behavior above T_m ($T \leq T_m$) may be related to liquid like ion transport in the amorphous phase of the host polymer matrix that is aided by the local chain mobility in the polymer backbone.

3.5. Electrochemical stability and ion transport results

The residual current as a function of applied dc bias for PS and PNCE films is presented in Fig. 12. This is the voltage stability of the samples under study observed in terms of the breakdown voltage. For the PS film, the increase in residual current is progressive (~nA range) until the applied voltage is around ~2.75 V, beyond which it rises suddenly by about three orders of magnitude (~μA range). A similar variation is observed for nanocomposite films. The voltage limit beyond which the residual electronic current rises to a very high value is indicative of the sample breakdown voltage (also known as the 'working voltage' limit). It sets a threshold

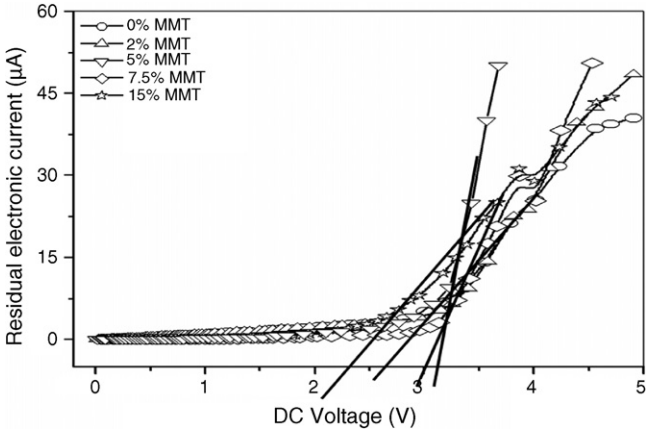

Fig. 12. Variation of residual electronic current as function of applied dc voltage for different organo-clay concentration (x = 0, 2, 5, 7.5, 15).

Table 5
Experimental values of ionic transport (t_{ion}), electronic transport (t_e) and voltage stability (breakdown voltage) for PNCE films.

Clay (wt.%)	Ionic transport number (%)	Electronic transport number (%)	Ionic conductivity (S cm^{-1})	Electronic conductivity (S cm^{-1})	Breakdown voltage (V)
0	99.9	0.1	4.4×10^{-7}	4.4×10^{-10}	2.75
2	99.9	0.1	6.1×10^{-5}	6.1×10^{-8}	2.85
7.5	99.9	0.1	3.1×10^{-5}	3.1×10^{-8}	3.0
15	99.7	0.3	3.7×10^{-5}	3.7×10^{-8}	2.4

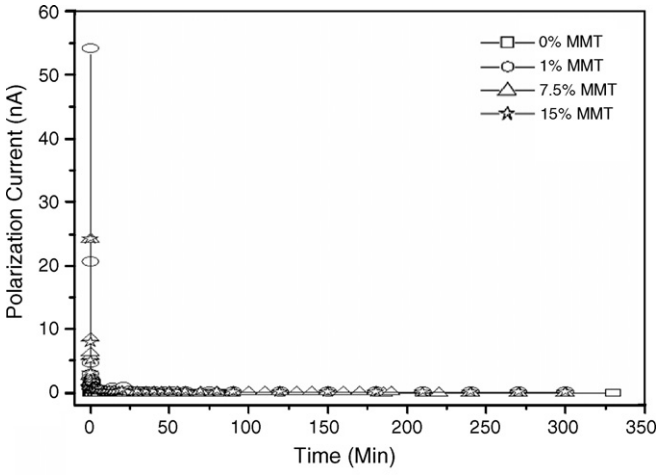

Fig. 13. Variation of polarization current as function of time under constant applied voltage (V = 50 mV) for different concentration (x = 0, 1, 7.5, 15) of DMMT clay.

limit of voltage stability for the ion-conducting polymer films, the value is obtained from the intercept of the tangent drawn over the non-linear portion of the current rise with the voltage axis. A voltage stability of 3.0 V is observed for the 7.5 wt.% clay composite in comparison with 2.75 V for the clay-free PS film. There is a clear improvement in the voltage stability factor in the PNCE films.

The ionic transport number, 't_{ion}', of selected compositions of the PNCE films has been measured using a dc polarization technique with a fixed applied voltage (i.e., 50 mV) across the sample cells (kept well within the electrochemical stability range). The variation in the polarization current as a function of time at a fixed dc is shown in Fig. 13. The results show a high initial current (I_T) followed by attainment of saturation current (I_e) after a few hours. The high value of the initial current is attributed to the combined contribution of both the ionic and the electronic components in the sample whereas the final saturation current is related to a steady-state current due to the mobility of electrons only [37]. The experimental values of I_T and I_e for different PNCE films enable separation of the ionic (t_{ion}) and electronic (t_e) components in the overall electrical transport in the sample films in accordance with the Eq. (1). The calculated value of the ion transport number (t_{ion}) for the clay-free PS film is 99.9% and is almost the same for PNCE films irrespective of clay concentration. Transport number data have also been used to estimate the ionic and electronic contribution to the electric conductivity for various clay concentrations in the PNCE films (Table 5). The electronic conductivity of the PNCE films is very much within the desirable limit ($\leq 10^{-7}$ S cm^{-1}) for its utility in device applications.

In addition to separate ionic (t_{ion}) and electronic (t_e) contribution to the electrical transport, the actual contribution of cations to the transport properties in PNCE films is estimated by means of a combined dc polarization/ac impedance measurement technique [38]. The cation transport number is calculated using the formula:

$$t_{Li^+} = \frac{I_s}{I_i}\left(\frac{\Delta V - I_i R_{i1}}{\Delta V - I_s R_{s2}}\right) \quad (5)$$

where ΔV is the applied dc bias, R_{i1} is the bulk resistance before polarization and R_{s2} is the resistance after polarization. The experimental value of Li^+ ion transport (t_{Li^+}), estimated from the results in accordance with Eq. (5) for a 2 wt.% clay-loaded PNCE film, is $t_{Li^+} \sim 0.50$. This value is very high, i.e., an enhancement by ~65% when compared with the corresponding value of $t_{Li^+} \sim 0.25$–0.30 for the clay-free PS, complexes, PEO_8LiClO_4 [39] and $PEO_{10}LiClO_4$ [40] reported by other workers.

4. Summary and conclusions

Intercalation-type polymer nanocomposite (PNCE) films have been prepared via incorporation of DMMT clay, arranged at the nanometer scale, into an ion conducting polymer matrix. The PNCE films show substantial enhancement in ambient temperature conductivity, reasonable improvements in stability properties (thermal/voltage), drastic increase in cation transport, and excellent correlation of electrical properties with the composite nanostructure. X-ray diffraction results confirm nanocomposite formation and intercalation of the cation-coordinated polymer chain with an optimized stoichiometric ratio of Ö/Li ~ 8 into the nanometric channels of organo-modified montmorillonite (DMMT) clay. The XRD observations appear to be in good agreement with TEM results. The latter micrographs clearly reveal the topography of the intercalated PNCE film with an enlarged clay gallery width ~18 Å for 20 wt.% loading of DMMT clay. The variation of dc conductivity with clay concentration appears to be well correlated with clay-dependent changes in the matrix phase structure expressed in terms of crystallinity fraction (X_c), T_g and T_m. Measurements of ion transport suggest that PNCE films have predominantly ionic character with convincing improvement in cation transport, voltage stability and thermal stability in comparison with the clay-free PS film. A substantial enhancement (~2 orders of magnitude) in dc conductivity at room temperature is displayed by clay-based PNCE films when compared with the clay-free polymer salt complex film. The improvement in the conductivity, stability and cation transport properties of the PNCE films suggests their suitability for energy storage devices such as: lithium polymer batteries and polymeric supercapacitor.

Acknowledgement

The authors acknowledge financial support received from Council of Scientific and Industrial Research (CSIR), New Delhi) vide sanction no. 03(1007)/04/EMR-II, Dated: 16.04.2004.

References

[1] P.E. Harvey, J. Power Sources 26 (1989) 23–32.
[2] W. Wieczorek, A. Zalewska, D. Raducha, Z. Florjanczyk, J.R. Stevens, A. Ferry, P. Jacobsson, Macromolecules 29 (1996) 143–155.
[3] M. Salomon, M. Xu, E.M. Eyring, S. Petrucci, J. Phys. Chem. 98 (1994) 8234–8244.
[4] W. Wieczorek, D. Raducha, A. Zalewska, J.R. Stevens, J. Phys. Chem. B 102 (1998) 8725–8731.
[5] P. Aranda, E.R. Hitzky, Acta Polym. 45 (1994) 59–67.
[6] E.P. Giannelis, Adv. Mater. 8 (1996) 29–35.
[7] E. Hackett, E. Manias, E.P. Giannelis, J. Chem. Phys. 108 (1998) 7410–7415.
[8] E. Hackett, E. Manias, E.P. Giannelis, Chem. Mater. 12 (2000) 2161–2167.
[9] P. Aranda, E.R. Hitzky, Chem. Mater. 4 (1992) 1395–1403.

[10] R.A. Vaia, K.D. Jandt, E.J. Kramer, E.P. Giannelis, Chem. Mater. 8 (1996) 2628–2635.
[11] R.A. Vaia, B.B. Sauer, O.K. Tse, E.P. Giannelis, J. Polym. Sci. B: Polym. Phys. 35 (1997) 59–67.
[12] R.A. Vaia, E.P. Giannelis, Macromolecules 30 (1997) 8000–8009.
[13] G. Sandí, R. Kizilel, K.A. Carrado, R.F. Saavedra, N. Castagnola, Electrochim. Acta 50 (2005) 3891–3896.
[14] G. Sandí, K.A. Carrado, H. Joachin, W. Lu, J. Prakash, J. Power Sources 119–121 (2003) 492–496.
[15] E.A. Stefanescu, P.J. Schexnailder, A. Dundigalla, I.I. Negulescu, G. Schmidt, Polymer 47 (2006) 7339–7348.
[16] S. Kim, E.J. Hwang, Y. Jung, M. Hana, S.J. Park, Colloids Surf. A: Physicochem. Eng. Aspects 313–314 (2008) 216–219.
[17] L. Fan, C.W. Nan, Z. Dang, Electrochim. Acta 47 (2002) 3541–3544.
[18] J.R. MaacCallum, C.A. Vincent, Polymer Electrolyte Reviews, vol. 1, Elsevier, Applied Science, London, 1987 (Chapter 1, pp. 5–8).
[19] P. Ferloni, G. Chiodelli, A. Magistris, M. Sanesi, Solid State Ionics 18–19 (1986) 265–270.
[20] P. Bala, B.K. Samantaray, S.K. Srivastava, Mater. Res. Bull. 35 (2000) 1717–1724.
[21] Dr. Roland Unger, Crystallization and phase behaviour in block copolymers of ethylene-oxide with tert.-butyl methacrylate and methyl methacrylate, Ph.D. Thesis, Technical University of Leuna-Mersebung, German, 1990.
[22] M.D. Mihaylova, V.P. Krestev, M.N. Kresteva, A. Amzil, I.V. Berlinova, Eur. Polym. J. 37 (2001) 233–239.
[23] Z. Shen, G.P. Simon, Y.B. Cheng, Eur. Polym. J. 39 (2003) 1917–1924.
[24] S. Kim, S.J. Park, Solid State Ionics 13–14 (2007) 973–979.
[25] B.L. Papke, M.A. Ratner, D.F. Shriver, J. Electrochem. Soc. 129 (1982) 1434–1438.
[26] T.D. Fornes, P.J. Yoon, D.L. Hunter, H. Keskkula, D.R. Paul, Polymer 43 (2002) 5915–5933.
[27] P. Meneghetti, S. Qutubuddin, Thermochim. Acta 442 (2006) 74–77.
[28] S. Pavlidou, C.D. Papaspyrides, Prog. Polym. Sci. 33 (2008) 1119–1198.
[29] S.S. Ray, M. Okamoto, Prog. Polym. Sci. 28 (2003) 1539–1641.
[30] S.A. Dutta, K. Bhowmick, P.G. Mukunda, T.K. Chaki, Polym. Degrad. Stabil. 50 (1995) 75–82.
[31] M. Zanetti, P. Bracco, L. Costa, Polym. Degrad. Stabil. 85 (2004) 657–665.
[32] B.N. Jang, C.A. Wilkie, Polymer 46 (2005) 3264–3274.
[33] S.R. Mohapatra, A.K. Thakur, R.N.P. Choudhary, J. Polym. Sci. B: Polym. Phys. 47 (2009) 60–71.
[34] A.K. Thakur, D.K. Pradhan, B.K. Samantaray, R.N.P. Choudhary, J. Power Sources 159 (2006) 272–276.
[35] X. Qian, N. Gu, Z. Cheng, X. Yang, E. Wang, S. Dong, Electrochim. Acta 46 (2001) 1829–1836.
[36] R.D. Marco, R. Eriksen, A. Zirino, Anal. Chem. 70 (1998) 4683–4689.
[37] C.J. Leo, A.K. Thakur, G.V. Subba Rao, B.V.R. Chowdari, J. Power Sources 115 (2003) 295–304.
[38] J. Evans, C.A. Vincent, P.G. Bruce, Polymer 28 (1987) 2324–2328.
[39] C.A. Vincent, Prog. Solid State Chem. 17 (1987) 145–261.
[40] M. Watanabe, Solid State Ionics 28–30 (1980) 911–917.